Inhibition of multi-species oral biofilm by bromide doped bioactive glass

M.E. Galarraga-Vinueza[1], B. Passoni[1], C. A. M. Benfatti[1], J. Mesquita-Guimarães[2], B. Henriques[1], R. S. Magini[1], M.C. Fredel[2], B. V. Meerbeek[3], W. Teughels[4], J. C. M. Souza[1,2*]

[1]Center for Education and Research on Dental Implants (CEPID), Post-Graduate Program in Dentistry (PPGO), Department of Dentistry (ODT), Federal University of Santa Catarina (UFSC), Florianópolis/SC, 88040-900, Brazil

[2]Ceramic and Composite Materials Research Group (CERMAT), Federal University of Santa Catarina, Florianópolis 88040-900, Brazil

[3]Dept. of Oral Health Sciences, BIOMAT, University Hospitals Leuven, Katholieke Universiteit Leuven, Kapucijnenvoer 33, Leuven B-3000, Belgium

[4]Dept. of Oral Health Sciences, University Hospitals Leuven, Katholieke Universiteit Leuven, Kapucijnenvoer 33, Leuven B-3000, Belgium

*Corresponding author:

Júlio César Matias de Souza, Prof Ph.D.

julio.c.m.souza@ufsc.br

Universidade Federal de Santa Catarina

Research Center on Dental Implants (CEPID)

Campus Trindade, Florianópolis, 88040-900, Brazil

Phone/Fax: +55 48 3721-9000

This article has been accepted for publication and undergone full peer review but has not been through the copyediting, typesetting, pagination and proofreading process which may lead to differences between this version and the Version of Record. Please cite this article as an 'Accepted Article', doi: 10.1002/jbm.a.36056

Abstract:

Bioactive glass is an attractive biomaterial that has shown excellent osteogenic and angiogenic effects for oral bone repairing procedures. However, anti-biofilm potential related to such biomaterial has not been completely validated, mainly against multi-species biofilms involved in early tissue infections. The aim of the present study was to evaluate the anti-biofilm effect of 58S bioactive glass embedding calcium bromide compounds at different concentrations. Bioactive glass containing 0, 5, or 10wt% $CaBr_2$ was synthesized by alkali sol-gel method and then characterized by physco-chemical and scanning electron microscopy (SEM)**.** Then, samples were tested by microbiological assays using optical density, real time q-PCR, and SEM. Bioactive glass particles showed accurate chemical composition and an angular shape with a bimodal size distribution ranging from 0.6 to 110 µm. The mean particle size was around 29 µm. A significant anti-biofilm effect was recorded for 5wt% $CaBr_2$-doped bioactive glass against *S. mitis, V. parvula, P. gingivais, S. gordoni, A. viscosus, F, nucleatum, P. gingivais. F. nucleatum* and *P. gingivalis.* Such species are involved in the biofilm structure related to infections on hard and soft tissues in the oral cavity. The incorporation of calcium bromide into bioactive glass can be a strategy to enhance the anti-biofilm potential of bioactive glasses for bone healing and infection treatment.

Key words: Bioactive glass, anti-biofilm, bromide, sol-gel synthesis, bone infection, bone healing

1. Introduction

Bioactive glass (BG) is a promising biomaterial developed 40 years ago by the American scientist Larry Hench who produced the first BG of 45S5 composition with the purpose of repairing human bone defects and derived infections [1,2]. Previous studies have widely shown the outstanding properties on 45S5 BG, such as stimulation of osteogenic cell migration, vascularization, dissolution in bone tissue, and antibacterial effects induced by ion release [3]. In the 90s, a bioactive glass named 58S was developed via sol-gel method, in order to obtain an alternative compound with similar properties to those recorded for 45S5. Sepulveda *et al*. showed that melt-derived 45S5 BG powders exhibited lower dissolution rates for hydroxyapatite formation in comparison to those on 58S sol gel-glass powder [4]. Accordingly, hydroxyapatite is fundamental for bone healing and remodeling. Thus, the formation of a carbonated hydroxyl-apatite (CHA) layer establishes a bioactive interface between bone and BG surface, mimicking the mineral phase of bone, that also induces osteogenic cell proliferation, resulting in a desired biological match between BG particles and human tissues [1,5,6].

Nonetheless, proper bioactive response is only one of the purposes of a bioactive material. Bone infection occurs in the range of 1-2.5% being an issue of orthopedic and oral surgeries [5,7,8]. In fact, biofilms are responsible for more than 80% of human infections [9,10] which influence the clinical use of antibiotics after surgical procedures. The antibacterial effect revealed by BG has been attributed to the ion release capability in increasing the pH of the surrounding medium that can affect planktonic bacteria growth [11]. Most of the studies report that the BG antibacterial effect against specific planktonic bacteria do not reflect realistic conditions of biofilm growth and

pathogenicity at infected areas [12–16]. Biofilm is a well-organized microbial community embedded in an extracellular polymeric matrix composed of polysaccharides, nucleic acids, proteins and water, that adheres to different surfaces such as teeth, rehabilitation synthetic materials, bone, and soft tissues [17,18]. As a result of a complex well-organized structure, bacteria embedded in biofilm is 1000 times more resistant to antibiotic therapy compared to planktonic bacteria [9,12]. Additionally, studies have shown that biofilm formation may enhance virulence of certain pathogenic bacteria like P. *gingivais* [19], S. *mitis,* F. *nucleatum,* A. *viscosus,* A. *actinomycetemcomitans,* and *V. parvula* [20].

In an attempt in improving BG antibacterial and anti-biofilm activity, several studies have reported positive antibacterial properties achieved by bioactive glasses embedded with inorganic compounds containing silver, cerium, selenium, magnesium, zinc, or fluoride [14,15,21–24]. Bromine, a chemical element corresponding to the halogen group, has been poorly explored in tissue engineering applications. One study reports the application of 12-methacryloyloxydodecylpyridinium bromide (MDPB) monomer as an antibacterial agent embedded in resinous biomaterials. That previous study reported an effective antibacterial and anti-biofilm activity of MDPB against *S. mutans* species over a period of 60 s. That was attributed to the inhibition of an enzyme named lactate dehydrogenase activity which is responsible for the *S. mutans* metabolism [25]. Nevertheless, there are no studies reporting the incorporation of $CaBr_2$-based compounds in BG composition to enhance its antibacterial activity. Therefore, the aim of the present study was to produce a bioactive glass embedding calcium bromide as an innovative strategy to inhibit biofilm formation avoiding infections at bone and

surrounding tissues. The null hypothesis of this study was that the presence of bromide does not affect the multi-species biofilm growth on 58S bioactive glass.

2. Materials and Methods

2.1. Preparation of $CaBr_2$-doped bioactive glass

The methodology applied in this study to synthesize and analyze 58S bioactive glass embedding $CaBr_2$ is represented in Figure 1. First, BG (58 wt% SiO_2, 33 wt% CaO, 9 wt% P_2O_5) powder was processed by sol-gel method following a previous study performed by the authors [26]. For that, tetraethyl orthosilicate (TEOS) (98%, Sigma Aldrich, USA), triethyl phosphate (TEP) (99.8%, Sigma Aldrich, USA) and calcium nitrate tetrahydrate ($Ca(NO_3)_2{\cdot}4H_2O$) (Vetec, Brazil) were used as precursors of silicon, phosphorous and calcium oxide, respectively. Nitric acid (HNO_3, 68%, Vetec, Brazil) was used to dissolve $Ca(NO_3)_2{\cdot}4H_2O$ and to adjust pH solution while ethyl alcohol (EtOH, P.A., Synth, Brazil) was used to dissolve TEOS and TEP. Molar ratio of SiO_2, P_2O_5 and CaO was calculated, concerning the BG58S proportion. TEOS and TEP were placed in a glass recipient containing EtOH under magnetic stirring at 25 ^{o}C for 10 min. $Ca(NO_3)_2{\cdot}4H_2O$ was dissolved in 2 M HNO_3 and then added to water at a molar ratio TEOS:H_2O of 1:4. For bromide doped BG58S samples, calcium bromide hydrate ($CaBr_2.xH_2O$, Sigma-Aldrich, USA) was added as bromide precursor to achieve 5 or 10 wt% $CaBr_2$. Considering the stoichiometric relation of calcium bromide, calcium nitrate quantity was calculated to maintain the final amount of 33wt% CaO. The mixtures were added to the solution and stirred for 1 h. Solution was placed in a chamber at 70 °C for drying over a period of 24 h. Subsequently, the material was thermally treated at 600 °C

and milled in planetarium ball mill (PM100, Retsch, Germany) at 400 rpm for 1 h, to obtain the bioactive glass powder.

BG powders were deagglomerated in a mortar agate with acetone. Then, BG powders were sieved at 106 µm and pressed at 80 MPa to obtain small discs of 10 mm diameter and 1 mm thickness. Thermal treatment was performed at 1150ºC, by 10 ºC/min heating rate and 180 min of holding time.

2.2. Physico-chemical and morphological analyses

An initial chemical analysis was performed by energy dispersive X-ray spectroscopy (EDX, Swift 2000, Hitachi, Japan). The compound composition was obtained by rearranging the quantity of oxygen to calculate the weight percentage of oxides using the most stable stoichiometric arrangement, resulting in a reliable tool to semi-quantify the respective oxides. To evaluate the density of the sintered samples, the Archimedes Principle was applied to measure the relative density of the discs in green and after thermal treatment at 1150 ºC.

The particle size distribution was measured in a laser diffraction equipment (Mastersizer 2000, Malvern, UK). The powder was introduced in a wet dispersion unit with low water rotation around 1200 rpm to avoid any deagglomeration of the sample. Before microbiological assays, the morphologic aspects of the BG particles as well as the surfaces of the test samples were analyzed by scanning electron microscopy (SEM), (TM3030, Hitachi, Japan) at 15 kV by back-scattering electron (BSE) mode. Samples were sputter-coated with gold prior to SEM analysis.

The roughness values of the disc samples were obtained regarding *Rt* (maximum height between peak and valley) and *Ra* roughness parameter that consists in the arithmetic mean value between the peak and valley height values in the effective roughness profile. The R*a* roughness was recorded at five different areas on each material (*n*=25) using an optical profilometer (Zygo, NewView, 7300, USA). The measurement length was 0.7 mm and cut off at 0.25 mm for 3 s. Afterwards, a color map and 3D model representation of the surface roughness was performed per each sample using the Mountain map Software (Digital Surf, France).

The X-ray diffraction (XRD) analysis was performed on the powder and thermal treated samples to evaluate the presence of crystalline phases in the amorphous matrix of the bioactive glass. The samples were analyzed in a diffractometer (D8 Discover, Bruker, Germany) by using Cu Kα radiation (λ = 1.5406 Å) on theta-2 theta mode. The range of analyzed angles was at 10-70º, with a step size of 0.04º and 1s of step time. The peaks for each phase were identified using X'Pert High Score Plus Software (Panalytical, USA) within JCPDS patterns database.

2.3. Biofilm growth conditions

Bioglass discs with different concentrations of $CaBr_2$ (0%, 5% or 10%), were tested against a multi-species biofilm, grown in a bioreactor (*BIOSTAT® B*, Germany) simulating the oral conditions as illustrated Figure 1. The multi-species form included 10 strains as follow: 2 early colonizer bacterial species *(Streptococcus mitis* and *Streptococcus gordonii*), 5 pathogen bacterial species (*Fusobacterium nucleatum, Porphyromonas gingivalis, Prevotella intermedia, Streptococcus mutans, Streptococcus*

sobrinus) and 3 beneficial bacterial species (*Veillonella parvula, Actinomyces viscosus, Streptococcus salivarius).*

750ml of BHI II [27] 37 g/L containing brain heart infusion broth, 2.5 g/L mucin from porcine stomach type III (Sigma-Aldrich Chemie GmbH, Buchs, Switzerland), 1g/L yeast extract, 0.1 g/L L-cysteine, 2 g/L sodium bicarbonate was added to the bioreactor vessel. Also, the calibration of pH electrode was performed with 1/10 HCl 1/10 and the 1 molar NaOCl before the sterilization process. Yet, one vessel of 2L was prepared with fresh BHI II, in order to be able to refresh the growth medium twice a day, over the experiment period. After the sterilization process, the bioreactor was set-up with 300 rpm of stirring on anaerobic condition at 37°C. Also, an anti-foam liquid was added before the overnight wait.

Bacterial strains were grown overnight at 37°C in BHI under aerobic or anaerobic conditions, as described in the ATCC recommendations for each strain and then incubated in the bioreactor. After 24 h, the bioreactor medium was supplemented with 5 mg/L hemin, 1 mg/L menadione, and the absorbance of medium was adjusted to zero. After this procedure, the absorbance of the bacterial suspension was controlled to achieve the same optical density values prior to incubation in the bioreactor. Stable multi-species biofilm were obtained for 72 h. After this period, BG discs were placed at the bottom of 24 well-plates. Each well containing a BG disc was filled-up with 900 µL fresh BHI and 100 µL bioreactor culture. The negative and positive control groups had pure bioglass discs. However, the negative control group received 900 µL fresh BHI and 100 µL bioreactor culture while the positive control group was tested with 400 µL chlorhexidine, 500 µL fresh BHI and 100 bioreactor culture.

The 24 well plates were incubated at 37°C under anaerobic conditions over a period of 24 h biofilm growth. Then, the supernatant was carefully removed with pipets, and therefore the discs were smoothly cleaned two times with 300 µL PBS to withdrawn the weakly attached biofilm. The well-attached biofilm was removed with 300 µL trypsin, into an anaerobic jar and maintained into the incubator for 15 min. The trypsin from each well was added to Eppendorf's to be centrifuged and then the pellets were re-suspended in 500 µL PBS. On such dilution, a vitality DNA extraction was performed using 10 µL PMA and 90 µL bacterial dilution in PBS. The real time q-PCR was performed in triplicate for each strain using the ABI 7700 Sequence Detection System platform (Applied Biosystems, Foster City, CA, USA) [28]. Data was exported to an excel sheet to analyze the amount of each strain into the biofilm.

For microscopic analyses, discs covered with biofilms were washed two times in PBS and fixed in glutaraldehyde 2% for 5 min. Then, discs were washed three times in PBS, and dehydrated through a series of graded ethanol solutions (50, 70, 80, 90, 100%). Samples covered with biofilms were sputter-coated with gold, and analyzed by scanning electron microscopy.

3. Results

3.1. Chemical and morphological analysis

The particle size distribution of BG58S particles revealed a bimodal distribution with particle size ranging from 0.6 up to 110 µm, as seen in Figure 2. The mean particle size was around 29 µm. The chemical composition of 58S BG powder particles was quite similar to the expected composition (58 ± 4 wt% SiO2, 33 ± 3 wt% CaO, 9 ± 2 wt%

P2O5), as detected by EDX analyses. The EDX spectra of all compositions are shown in Figure 3.

The EDX spectra showed the highest intensity peak for Si element. The intensity of Ca element is intermediary while the peak for P element was the lowest in the spectra. Furthermore, the bioactive glasses embedding $CaBr_2$ revealed an increase in the Br peak with the increase of $CaBr_2$ in the composition.

XRD spectra for the powders and heat pressed 58S bioactive glass samples free of $CaBr_2$ are shown in Figure 4 while XRD spectra for samples embedding $CaBr_2$ are shown in Figures 5 and 6.

The XRD spectra of the bioactive glass powders revealed a broad diffraction band, confirming its amorphous and glassy nature [4,31,32]. Moreover, peaks of tetracalcium phosphate (TTCP), dicalcium silicate (DCS) and bromine oxide were identified that confirmed the success of the modified sol-gel synthesis. The increase of bromine phases was noticed with increasing of the amount of $CaBr_2$ in the bioactive glass composition. Considering the crystalline phases, XRD peaks for calcium phosphate phases, wollastonite, pseudowollastonite and quartz were detected as tresult from the high heat treatment [32–36]. Pseudowollastonite is a polymorph of wollastonite, that possesses a transition temperature around 1250 ºC. However, the excess of SiO_2 favors the formation of the pseudowollastonite at lower temperatures [35,36].

In the case of the XRD spectra for BG58S 5%$CaBr_2$, the crystalline phases of quartz, tricalcium phosphate, wollastonite and phosphorus bromide were detected after 1150 ºC. The increase in the crystallization intensity of quartz can be explained by the decomposition of dicalcium silicate, in CaO and SiO_2 [35,36]. Phosphorus bromide

crystallizes from the decomposition of tetracalcium phosphate into β-tricalcium phosphate, releasing phosphates to react with bromine oxide [35,36].

In the case of the XRD spectra recorded for BG58S 10%$CaBr_2$, calcium phosphate silicate, pseudowollastonite, wollastonite and silicon bromide phases were detected after thermal treatment at 1150 ºC. That indicated that the silicon was not available to crystallize alone and therefore it reacted almost on totality with the bromine oxide to crystallize silicon bromide. That can be associated with the excess of $CaBr_2$ in such chemical composition. However, the thermal treatment promoted the formation of pseudowollastonite and wollastonite [32,35,36].

SEM images revealed 58S bioactive glass powder containing angular shape morphology that is typical from glass milling procedure. However, BG58S samples containing 5%$CaBr_2$ before thermal treatment revealed needle like crystals typical from calcium phosphate phases [29] before thermal treatment. Such crystals disappeared and formed angular lighter crystals like β-Tricalcium phosphate after thermal treatment at 1150 ºC [30]. Surfaces of bromide-doped 58S BG discs revealed a rough morphologic aspect associated with the content of $CaBr_2$. Thus, the presence of CaB_2 seemed to affect the densification process of the bioactive glass. Thermal treatment performed at a higher temperature and longer holding time should promote an increase in atomic diffusion rates, leading to the formation of larger and structural ordered particles. The morphological aspects of the 58S BG particles and discs are shown in Figure 4.

The arithmetic average roughness (*Ra*) values and maximum height between peak and valley values (*Rt*) recorded on 58S BG discs increased with $CaBr_2$ content as shown and illustrated in Figure 5.

The relative density of the samples were determined via Archimedes method before and after thermal treatment. Several thermal cycles were assessed at maximum temperature ranging from 600 up to 1250 ^{o}C in order to achieve a high density for the samples. A proper maximum temperature at 1150 ºC of thermal treatment was selected considering final shape and high density for microbiological assays. The relative density of the samples before the thermal treatment was higher than 50%. Additionally, the relative density of those samples increased with the $CaBr_2$ content. In a similar way, the sintered samples had a relative density of more than 74%, which increased directly with the $CaBr_2$ content, achieving around 95% relative density on the highest concentration of $CaBr_2$ (Figure 5).

3.2. Biofilm Inhibition

A significant biofilm inhibition, represented by the decrease of bacterial cell amount, was noticed when the chlorhexidine was placed in contact with the multi-species biofilm grown on the 58SBG discs free of $CaBr_2$. That validated the antimicrobial effect of chlorhexidine against all the early, beneficial and pathogenic species tested in this study. The amount of bacteria also decreased in the presence of 58SBG discs doped with 5% $CaBr_2$ regarding *S. mitis* and *S. gordonii* (early colonizers), *V. parvula* and *A. viscosus* (beneficial species), and *P. gingivalis* (pathogenic species). However, no decrease of bacterial amount was detected for multi-species biofilm grown on 58S BG discs doped with 10wt% $CaBr_2$. Results of biofilm inhibition obtained by q-PCR analyses for early, beneficial, and pathogen bacteria are shown in Figures 6 and 7.

SEM inspection of the 58S BG discs surfaces covered with multi-species biofilms is shown in Figure 8. Considering the morphology of the multi-species biofilm tested in

the present study, streptococcus, bacillus, and filamentous species can be detected on bioactive glass surfaces free or containing $CaBr_2$ after 24h of multi-species biofilm growth (Fig. 8). The multi-species biofilm revealed similar morphological aspects on all the test samples inspected by SEM.

4. Discussion

The present study incorporated calcium bromide as a potential anti-biofilm compound into BG composition, which for the first time has been explored in tissue engineering applications. Accordingly, the results of this study has supported the hypothesis that BG modified with calcium bromide is able to inhibit different bacteria in multi-species oral biofilm revealed by real time q-PCR analysis. This study demonstrated an appropriate chemical and bimodal size distribution of BG particles and therefore BG samples embedding 5wt% $CaBr_2$ had an anti-biofilm effect against early and pathogen oral biofilm species.

In the present study, BG embedding 5wt% $CaBr_2$ had a notorious anti-biofilm effect against species such as *S. mitis, S. gordonii, A. viscosus, V. parvula,* and, *P. gingivalis*. Conversely, no biofilm inhibition was noted for BG samples embedding 10wt% $CaBr_2$, probably due to the higher roughness values revealed by the discs surfaces corresponding to this experimental group. A high roughness seemed to affect negatively the anti-biofilm potential. Previous studies have reported that surfaces with higher roughness have more compatibility with biofilm adherence because bacteria is sheltered against shear forces. Additionally, biofilm adhesion area increases with the increase of roughness that allow the accumulation of biofilm [39–41]. SEM analysis of biofilm adherence in the disk samples of this study did not show differences between the control

and experimental groups; nevertheless, this is a qualitative analysis which only reveals the presence of certain species an is not as precise as q-PCR analysis.

Furthermore, tissue engineering has been challenged to improve BG chemical composition considering biocompatibility and antibacterial effects. In the present study, the crystalline phases analysis revealed the presence of bioactive phases for bone healing such as tetracalcium phosphate and dicalcium silicate [32,34,37]. Regarding BG58S 5%$CaBr_2$ processed at 1150 ºC, the XRD spectra (Fig 5) also revealed the presence of phosphorus bromide. Phosphorus tribromide is a compound used in pharmacology as an active ingredient of anti-inflammatory, analgesic and antipyretic reactions. Also, BG58S 5%$CaBr_2$ presented the crystal microstructures typical from calcium phosphates phases, which is an indication of a high bioactive ability.

Several previous studies have shown suitable antibacterial properties achieved by bioactive glasses doped with diverse oxides [10-12]. However, possible toxic effects caused by metallic ions and particles embedded into BG are still a controversial concern for clinical applications. Most studies have tested antibacterial properties of modified bioactive glasses against planktonic bacteria solely [7,15,42]. Goh *et al*. reported that BG samples modified with 5 and 10 mol% cerium oxide demonstrated a significant antibacterial activity against *E. coli,* evaluated by the quantitative viable count method [14]. Additionally, El-Kady *et al*. established in their study that all BG nanoparticles doped with 1, 3, 5, and 10wt% Ag_2O had antibacterial effect against S. *aureus* and E. *coli* cultures evaluated by the disk diffusion method. That study attributed the high effective antibacterial effect to the presence of silver ions [13]. In contrast, Fooladi *et al*. stated that silver is not an essential component for inhibiting bacterial growth [24]. That study incorporated MgO into BG nanopowders and its antibacterial effect was assessed

against *E. coli, P.aureginosa*, and *S. aureus*. The BG nanopowders at a greater concentration than 15.62 mg/mL showed efficient inhibitory effects on the three bacterial strains. As well, selenium nanoparticles have also being added to BG as an antibacterial agent. Stevanovic *et al*. showed in their study that BG 45S5 with selenium nanoparticles had a significant antibacterial activity against *S. aureus* and *S. epidermis* cultures, and inhibited *B. subtilis* and *K. pnuemoniae* growth [23]. Fluorine has also being added to BG particles as an antimicrobial agent. Xu *et al*. showed in their study that BG particles mixed with sodium fluoride (NaF) had a significant *S. mutans* biofilm inhibition effect after 24 hours of exposure. That study tested the anti-biofilm effect against one oral bacteria (monospecie biofilm); nevertheless, there are not enough studies testing modified bioactive glass against multi-species oral biofilms. Fluorides are known to inhibit bacterial enzymes like enolase and catalase. Also, compounds with fluorine may disrupt bacterial cell membranes and cytoplasm pH, and interfere glycolysis of cariogenic bacteria [15]. Bromine has many similar characteristics to fluorine although bromine has not being incorporated into BG composition as an anti-biofilm agent in previous studies. Considering a lack of findings on the effect of Br-based compounds, this study pursued the objective of testing bromide doped BG as a new repairing biomaterial to inhibit multispecies oral biofilm.

The results of the present study are promising since bromide had an anti-biofilm effect against early, beneficial, and pathogen oral species. Nevertheless, future studies evaluating anti-biofilm properties of $CaBr_2$ doped BG samples should take in consideration that samples characteristics, such as surface roughness are of extreme importance regarding biofilm adherence. One limitation of the present study was that

samples of the tested groups had different surface roughness values; consequently, biofilm inhibition was evaluated under different circumstances in each study group.

In addition, forthcoming studies should evaluate the biocompatibility and the hydroxyapatite formation capability of innovative bromide doped BG to be tested in future *in vivo* studies. Regarding the mechanism in which bromine acts as anti-biofilm agent, new studies should analyze how bromine ions are able to affect biofilm formation and additionally include clinical strains isolated from patients reporting infection in implanted sites to mimic conditions that are more realistic to clinical complications.

5. Conclusions

Within the limitations of this study, the main outcomes of this work are drawn as follow:

- The chemical composition of the $CaBr_2$-doped bioactive was monitored and therefore the powder particles showed an angular shape and bimodal size distribution. That plays an important role on the clinical application in bone defects;
- Considering microbiological assessment, bioactive glass doped with 5wt% $CaBr_2$ had a considerable anti-biofilm effect against oral bacteria involved in a multi-species biofilm. Such findings are more representative concerning the aggregation pathways among different species when compared to mono-species methods related in literature. In fact, biomaterials embedding potential anti-biofilm compounds must be tested against multi-species biofilms as reported in the present study
- $CaBr_2$-doped bioactive glass can be considered an advantageous anti-biofilm biomaterial for clinical applications and treatment of oral infections at implanted

surgical sites. Notwithstanding, other bromide contents and compositions should be assessed by physicochemical and biological tests in further studies to clarify the anti-biofilm behavior of such enhanced bioactive glasses.

References

[1] J.R. Jones, Review of bioactive glass: From Hench to hybrids, Acta Biomaterialia. 9 (2013) 4457–4486. doi:10.1016/j.actbio.2012.08.023.

[2] L.L. Hench, J.R. Jones, Bioactive Glasses: Frontiers and Challenges., Frontiers in Bioengineering and Biotechnology. 3 (2015) 194. doi:10.3389/fbioe.2015.00194.

[3] A. Hoppe, N.S. Güldal, A.R. Boccaccini, A review of the biological response to ionic dissolution products from bioactive glasses and glass-ceramics, Biomaterials. 32 (2011) 2757–2774. doi:10.1016/j.biomaterials.2011.01.004.

[4] P. Sepulveda, J.R. Jones, L.L. Hench, In vitro dissolution of melt-derived 45S5 and sol-gel derived 58S bioactive glasses., Journal of Biomedical Materials Research. 61 (2002) 301–11. doi:10.1002/jbm.10207.

[5] H. Wang, S. Zhao, X. Cui, Y. Pan, W. Huang, S. Ye, S. Luo, M.N. Rahaman, C. Zhang, D. Wang, Evaluation of three-dimensional silver-doped borate bioactive glass scaffolds for bone repair: Biodegradability, biocompatibility, and antibacterial activity, Journal of Materials Research. 30 (2015) 2722–2735. doi:10.1557/jmr.2015.243.

[6] M.N. Rahaman, B.S. Bal, W. Huang, Review: emerging developments in the use of bioactive glasses for treating infected prosthetic joints., Materials Science & Engineering. C, Materials for Biological Applications. 41 (2014) 224–31. doi:10.1016/j.msec.2014.04.055.

[7] A.M. El-Kady, A.F. Ali, R.A. Rizk, M.M. Ahmed, Synthesis, characterization and microbiological response of silver doped bioactive glass nanoparticles, Ceramics International. 38 (2012) 177–188. doi:10.1016/j.ceramint.2011.05.158.

[8] Z.-P. Xie, C.-Q. Zhang, C.-Q. Yi, J.-J. Qiu, J.-Q. Wang, J. Zhou, In vivo study

effect of particulate Bioglass® in the prevention of infection in open fracture fixation, Journal of Biomedical Materials Research - Part B Applied Biomaterials. 90 (2009) 195–201. doi:10.1002/jbm.b.31273.

[9] D. Davies, Understanding biofilm resistance to antibacterial agents., Nature Reviews. Drug Discovery. 2 (2003) 114–22. doi:10.1038/nrd1008.

[10] A. Dongari-Bagtzoglou, Pathogenesis of mucosal biofilm infections: challenges and progress., Expert Review of Anti-Infective Therapy. 6 (2008) 201–8. doi:10.1586/14787210.6.2.201.

[11] M. Gubler, T.J. Brunner, M. Zehnder, T. Waltimo, B. Sener, W.J. Stark, Do bioactive glasses convey a disinfecting mechanism beyond a mere increase in pH?, International Endodontic Journal. 41 (2008) 670–678. doi:10.1111/j.1365-2591.2008.01413.x.

[12] M.E. Olson, H. Ceri, D.W. Morck, A.G. Buret, R.R. Read, Biofilm bacteria: Formation and comparative susceptibility to antibiotics, Canadian Journal of Veterinary Research. 66 (2002) 86–92.

[13] A.M. El-Kady, A.F. Ali, R.A. Rizk, M.M. Ahmed, Synthesis, characterization and microbiological response of silver doped bioactive glass nanoparticles, Ceramics International. 38 (2012) 177–188. doi:10.1016/j.ceramint.2011.05.158.

[14] Y.F. Goh, A.Z. Alshemary, M. Akram, M.R. Abdul Kadir, R. Hussain, In-vitro characterization of antibacterial bioactive glass containing ceria, Ceramics International. 40 (2014) 729–737. doi:10.1016/j.ceramint.2013.06.062.

[15] Y.-T. Xu, Q. Wu, Y.-M. Chen, R.J. Smales, S.-Y. Shi, M.-T. Wang, Antimicrobial effects of a bioactive glass combined with fluoride or triclosan on Streptococcus mutans biofilm., Archives of Oral Biology. 60 (2015) 1059–1065. doi:10.1016/j.archoralbio.2015.03.007.

[16] M.E. Galarraga-Vinueza, J. Mesquita-Guimarães, R.S. Magini, J.C.M. Souza, M.C. Fredel, A.R. Boccaccini, Anti-biofilm properties of bioactive glasses embedding organic active compounds, Journal of Biomedical Materials Research Part A. (2016) 672–679. doi:10.1002/jbm.a.35934.

[17] J.C.M. Souza, R.R.C. Mota, M.B. Sordi, B. Bernardo, Biofilm Formation on Different Materials Used in Oral Rehabilitation, 27 (2016) 141–147. doi:10.1590/0103-6440201600625.

[18] J.G. Xavier, T.C. Geremias, J.F.D. Montero, B.R. Vahey, C.A.M. Benfatti, J.C.M. Souza, R.S. Magini, A.L. Pimenta, Lactam inhibiting Streptococcus mutans growth on titanium, Materials Science & Engineering C. 68 (2016) 837–841. doi:10.1016/j.msec.2016.07.013.

[19] S. Clais, G. Boulet, M. Kerstens, T. Horemans, W. Teughels, M. Quirynen, E. Lanckacker, I. De Meester, A.-M. Lambeir, P. Delputte, L. Maes, P. Cos, Importance of biofilm formation and dipeptidyl peptidase IV for the pathogenicity of clinical Porphyromonas gingivalis isolates., Pathogens and Disease. 70 (2014) 408–13. doi:10.1111/2049-632X.12156.

[20] F. Carrouel, S. Viennot, J. Santamaria, P. Veber, D. Bourgeois, Quantitative Molecular Detection of 19 Major Pathogens in the Interdental Biofilm of Periodontally Healthy Young Adults., Frontiers in Microbiology. 7 (2016) 840. doi:10.3389/fmicb.2016.00840.

[21] O. Lysenko, O. Dubok, A. Borysenko, O. Shinkaruk, The biological properties of the silver- and copper-doped ceramic biomaterial, Journal of Nanoparticle Research. 17 (2015). doi:10.1007/s11051-015-2971-z.

[22] V. Anand, K.J. Singh, K. Kaur, Evaluation of zinc and magnesium doped 45S5 mesoporous bioactive glass system for the growth of hydroxyl apatite layer, Journal of Non-Crystalline Solids. 406 (2014) 88–94. doi:10.1016/j.jnoncrysol.2014.09.050.

[23] M. Stevanović, N. Filipović, J. Djurdjević, M. Lukić, M. Milenković, A. Boccaccini, 45S5Bioglass®-based scaffolds coated with selenium nanoparticles or with poly(lactide-co-glycolide)/selenium particles: Processing, evaluation and antibacterial activity, Colloids and Surfaces B: Biointerfaces. 132 (2015) 208–215. doi:10.1016/j.colsurfb.2015.05.024.

[24] A.A. Imani Fooladi, H.M. Hosseini, F. Hafezi, F. Hosseinnejad, M.R. Nourani, Sol-gel-derived bioactive glass containing SiO2-MgO-CaO-P 2O5 as an

antibacterial scaffold, Journal of Biomedical Materials Research - Part A. 101 A (2013) 1582–1587. doi:10.1002/jbm.a.34464.

[25] N. Izutani, S. Imazato, K. Nakajo, N. Takahashi, Y. Takahashi, S. Ebisu, R.R.B. Russell, Effects of the antibacterial monomer 12-methacryloyloxydodecylpyridinium bromide (MDPB) on bacterial viability and metabolism., European Journal of Oral Sciences. 119 (2011) 175–81. doi:10.1111/j.1600-0722.2011.00817.x.

[26] J. Mesquita-Guimaraes, M.A. Leite, J.C.M. Souza, B. Henriques, F.S. Silva, D. Hotza, A.R. Boccaccini, M.C. Fredel, Processing and strengthening of 58S bioactive glass-infiltrated titania scaffolds, Journal of Biomedical Materials Research - Part A. (2016) 590–600. doi:10.1002/jbm.a.35937.

[27] G. Alvarez, M. González, S. Isabal, V. Blanc, R. León, Method to quantify live and dead cells in multi-species oral biofilm by real-time PCR with propidium monoazide., AMB Express. 3 (2013) 1. doi:10.1186/2191-0855-3-1.

[28] Qiagen, PCR Protocols & Applications - QIAGEN, (n.d.).

[29] L.R. Rodrigues, M.S. De Laranjeira, M.H. Fernandes, F.J. Monteiro, C.A. De Carvalho Zavaglia, HA/TCP scaffolds obtained by sucrose crystal leaching method: Preliminary in vitro evaluation, Materials Research. 17 (2014) 811–816. doi:10.1590/S1516-14392014005000082.

[30] Z. Sheikh, S. Najeeb, Z. Khurshid, V. Verma, H. Rashid, M. Glogauer, Biodegradable materials for bone repair and tissue engineering applications, Materials. 8 (2015) 5744–5794. doi:10.3390/ma8095273.

[31] S. Joughehdoust, S. Manafi, Synthesis and in vitro investigation of sol-gel derived bioglass-58S nanopowders, Materials Science-Poland. 30 (2012) 45–52. doi:10.2478/s13536-012-0007-2.

[32] M. Taghian Dehaghani, M. Ahmadian, M. Fathi, Synthesis, Characterization, and Bioactivity Evaluation of Amorphous and Crystallized 58S Bioglass Nanopowders, International Journal of Applied Ceramic Technology. 874 (2014) 867–874. doi:10.1111/ijac.12293.

[33] M. a. Encinas-romero, S. Aguayo-Salinas, S.J. Castillo, F.F. Castillón-Barraza, V.M. Castaño, Synthesis and characterization of hydroxyapatite-wollastonite composite powders by sol-gel processin, International Journal of Applied Ceramic Technology. 5 (2008) 401–411. doi:10.1111/j.1744-7402.2008.02212.x.

[34] M.A. Encinas-romero, J. Peralta-haley, J.L. Valenzuela-garcía, Synthesis and Structural Characterization of Produced by an Alternative Sol-Gel Route, 2013 (2013) 327–333.

[35] O.M. Goudouri, X. Chatzistavrou, E. Kontonasaki, N. Kantiranis, L. Papadopoulou, K. Chrissafis, K.M. Paraskevopoulos, Study of the Bioactive Behavior of Thermally Treated Modified 58S Bioactive Glass, Key Engineering Materials. 396–398 (2009) 131–134. doi:10.4028/www.scientific.net/KEM.396-398.131.

[36] M.M. Obeid, Crystallization of Synthetic Wollastonite Prepared from Local Raw Materials, International Journal of Materials and Chemistry. 4 (2014) 79–87. doi:10.5923/j.ijmc.20140404.01.

[37] W. Lu, W. Duan, Y. Guo, C. Ning, Mechanical properties and in vitro bioactivity of Ca5(PO4)2SiO4 bioceramic., Journal of Biomaterials Applications. 26 (2012) 637–50. doi:10.1177/0885328210383599.

[38] P. Gao, H. Zhang, Y. Liu, B. Fan, X. Li, X. Xiao, P. Lan, M. Li, L. Geng, D. Liu, Y. Yuan, Q. Lian, J. Lu, Z. Guo, Z. Wang, Beta-tricalcium phosphate granules improve osteogenesis in vitro and establish innovative osteo-regenerators for bone tissue engineering in vivo., Scientific Reports. 6 (2016) 23367. doi:10.1038/srep23367.

[39] W. Teughels, N. Van Assche, I. Sliepen, M. Quirynen, Effect of material characteristics and/or surface topography on biofilm development., Clinical Oral Implants Research. 17 Suppl 2 (2006) 68–81. doi:10.1111/j.1600-0501.2006.01353.x.

[40] M. Quirynen, C.M. Bollen, The influence of surface roughness and surface-free energy on supra- and subgingival plaque formation in man. A review of the literature., Journal of Clinical Periodontology. 22 (1995) 1–14.

[41] C.M. Bollen, P. Lambrechts, M. Quirynen, Comparison of surface roughness of oral hard materials to the threshold surface roughness for bacterial plaque retention: a review of the literature., Dental Materials : Official Publication of the Academy of Dental Materials. 13 (1997) 258–69.

[42] Y.-F. Goh, A.Z. Alshemary, M. Akram, M.R. Abdul Kadir, R. Hussain, Bioactive Glass: An In-Vitro Comparative Study of Doping with Nanoscale Copper and Silver Particles, International Journal of Applied Glass Science. 5 (2014) 255–266. doi:10.1111/ijag.12061.

Figure legends:

Figure 1. Schematic diagram showing the followed methodology to assess biofilm inhibition.

Figure 2. 58S BG Bimodal particle size distribution.

Figure 3. EDX spectra recorded for 58S bioactive glass free of $CaBr_2$ and including 5 or 10% $CaBr_2$.

Figure 4. XRD spectra recorded for 58S bioactive glass samples free of $CaBr_2$ processed at 600 or 1150 ^oC.

Figure 5. XRD spectra recorded for 58S bioactive glass samples embedding 5% $CaBr_2$ processed at 600 or 1150 ^oC.

Figure 6. XRD spectra recorded for 58S bioactive glass samples embedding 10% $CaBr_2$ processed at 600 or 1150 ^oC.

Figure 7. SEM images of BG 58S 5wt% $CaBr_2$ doped powder (A and B), BG 58S discs before thermal treatment (C) 0, (E) 5, and (G) 10 wt% Br and (D) 0, (F) 5, and (H) 10 wt% $CaBr_2$ BG 58S discs after thermal treatment up to 1150^oC.

Figure 8. *Ra, Rt* roughness values, color map and 3D representation of surface roughness for 0, 5, and 10wt% $CaBr_2$ doped 58S BG discs after thermal treatment up to 1150^oC.

Figure 9. Relative densities of green and sintered discs of BG 58S containing or not 5wt% or 10wt% $CaBr_2$.

Figure 10. Inhibition of early and beneficial oral biofilm species on 0wt% $CaBr_2$ 58S BG discs with chlorhexidine (CHX) (positive control group), 0wt% $CaBr_2$ BG58S discs (negative control group), 5 or 10 wt% $CaBr_2$ BG58S discs.

Figure 11. Inhibition of pathogen oral biofilm species on 0wt% $CaBr_2$ BG58S discs with chlorhexidine (CHX) (positive control group), 0wt% $CaBr_2$ BG58S discs (negative control group), and 5, 10 wt% $CaBr_2$ BG58S discs.

Figure 12. SEM images of multi-species biofilm adherence on BG58S discs with 0wt%$CaBr_2$ (A,B), 5wt% $CaBr_2$(C,D) and 10 wt% $CaBr_2$(E,F).

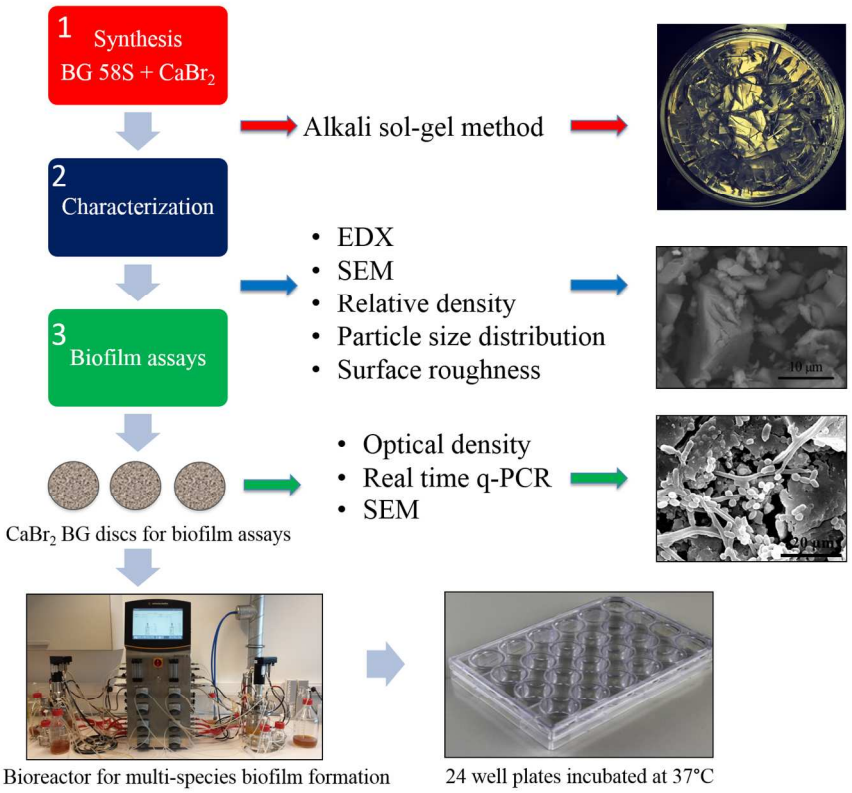

Figure 1. Schematic diagram showing the followed methodology to assess biofilm inhibition.

153x123mm (300 x 300 DPI)

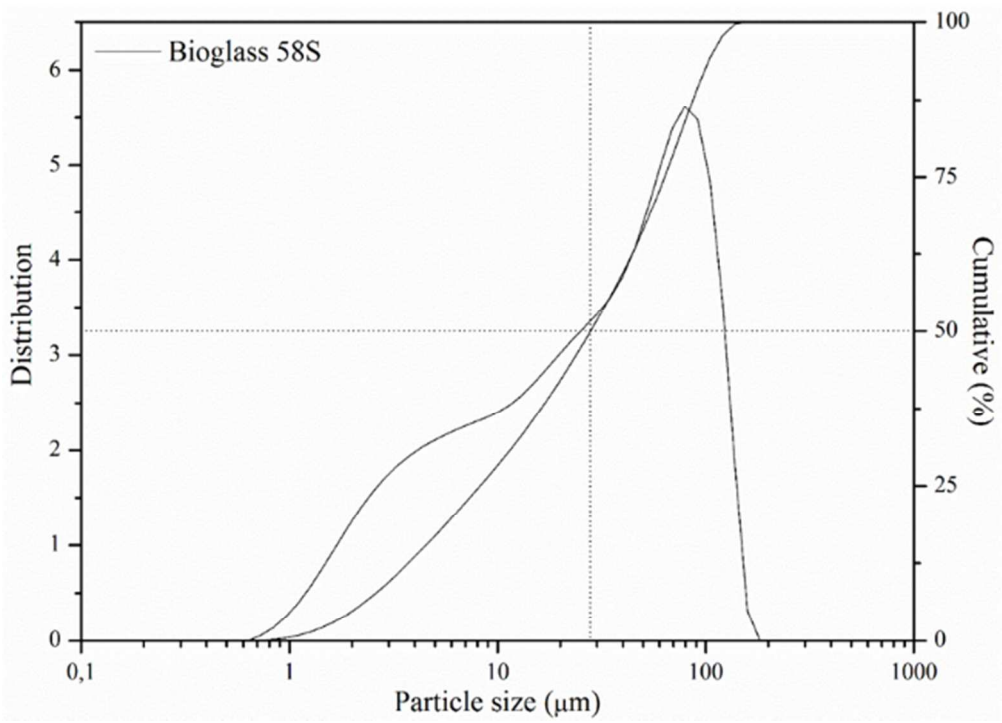

Figure 2. 58S BG Bimodal particle size distribution

55x39mm (300 x 300 DPI)

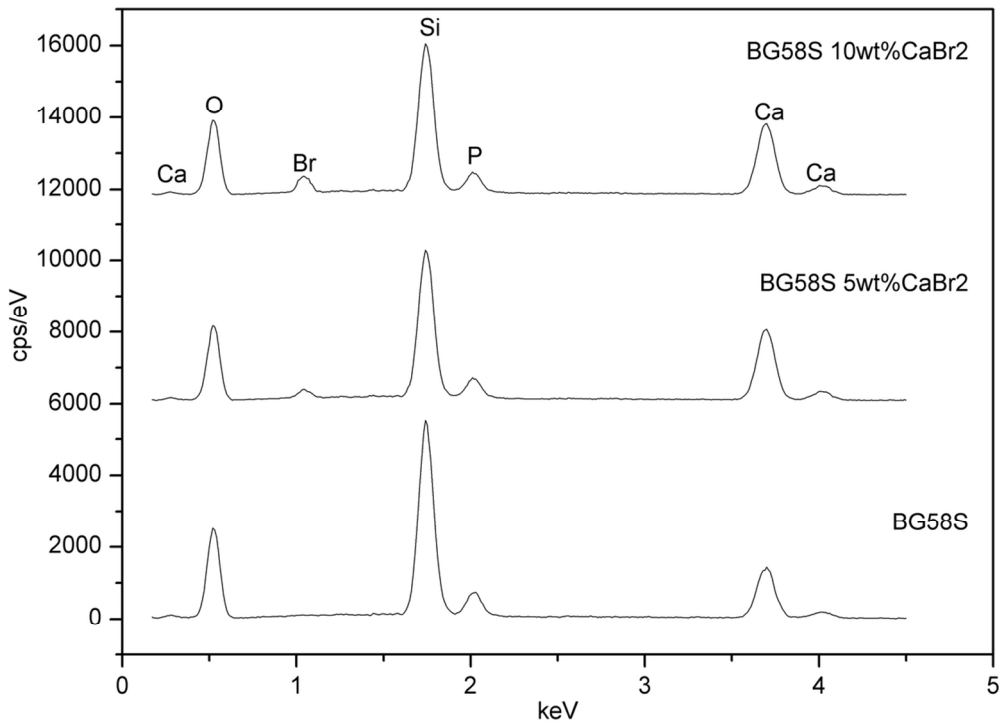

Figure 3. EDX spectra recorded for 58S bioactive glass free of CaBr2 and including 5 or 10% CaBr2.

105x76mm (300 x 300 DPI)

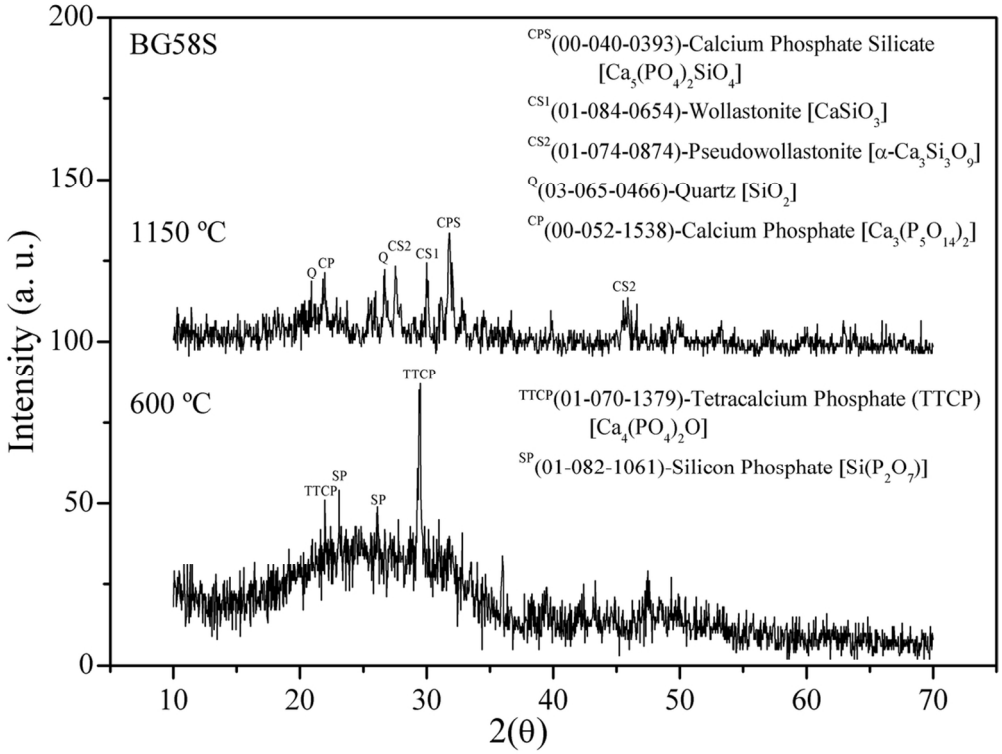

Figure 4. XRD spectra recorded for 58S bioactive glass samples free of CaBr2 processed at 600 or 1150 oC.

105x80mm (300 x 300 DPI)

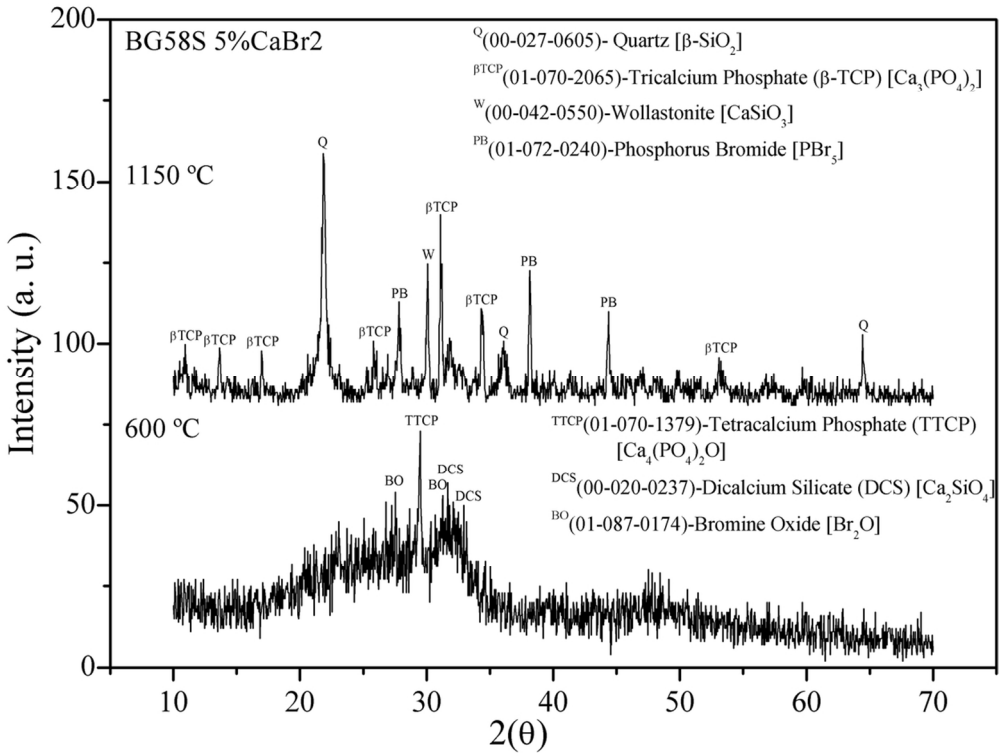

Figure 5. XRD spectra recorded for 58S bioactive glass samples embedding 5% CaBr2 processed at 600 or 1150 oC.

105x80mm (300 x 300 DPI)

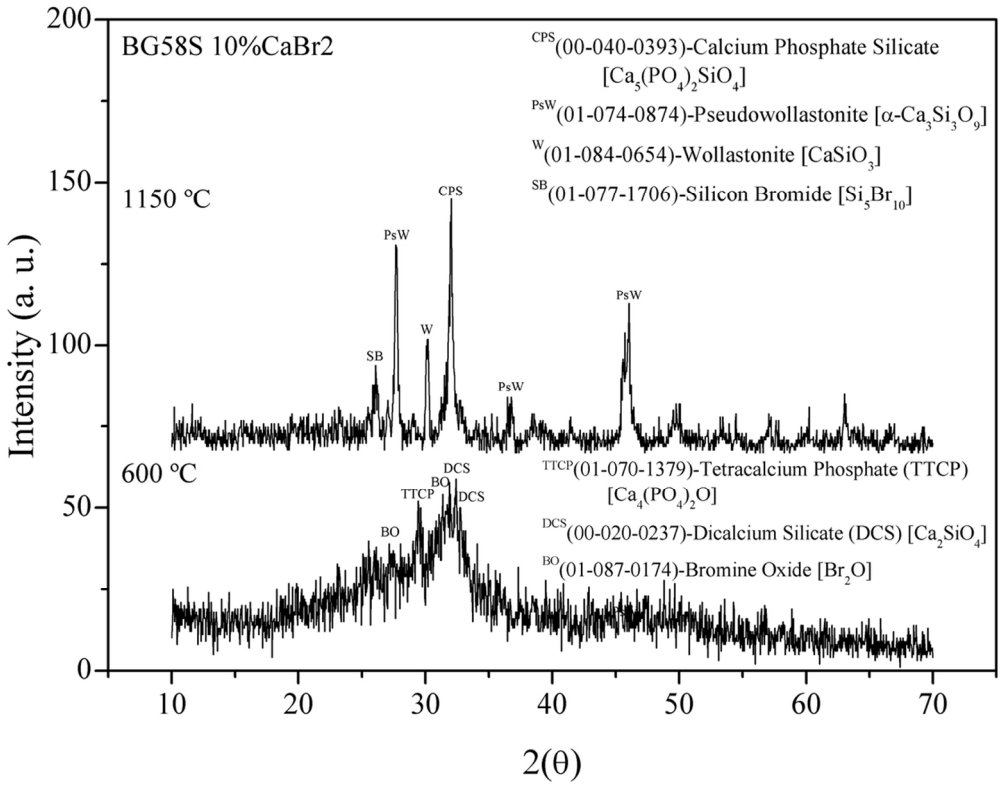

Figure 6. XRD spectra recorded for 58S bioactive glass samples embedding 10% CaBr2 processed at 600 or 1150 oC.

105x83mm (300 x 300 DPI)

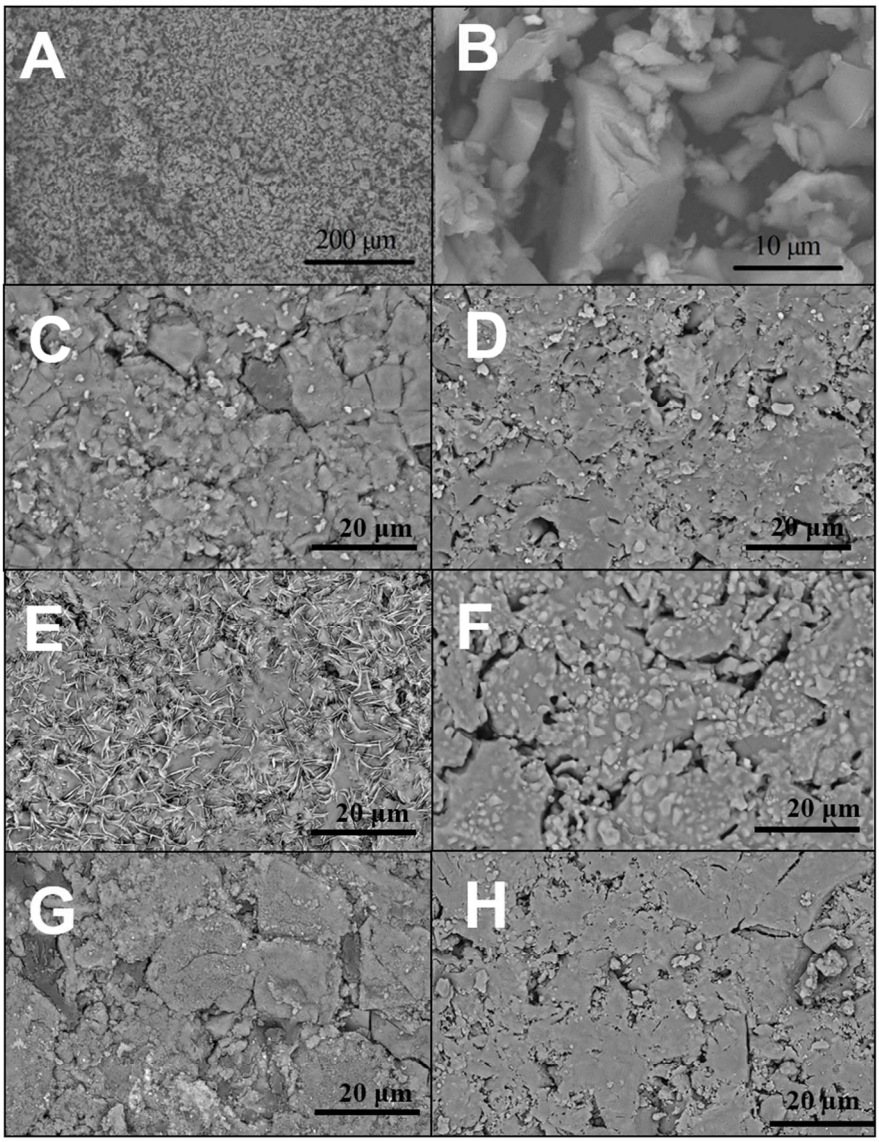

Figure 7. SEM images of BG 58S 5wt% CaBr2 doped powder (A and B), BG 58S discs before thermal treatment (C) 0, (E) 5, and (G) 10 wt% Br and (D) 0, (F) 5, and (H) 10 wt% CaBr2 BG 58S discs after thermal treatment up to 1150oC.

80x106mm (300 x 300 DPI)

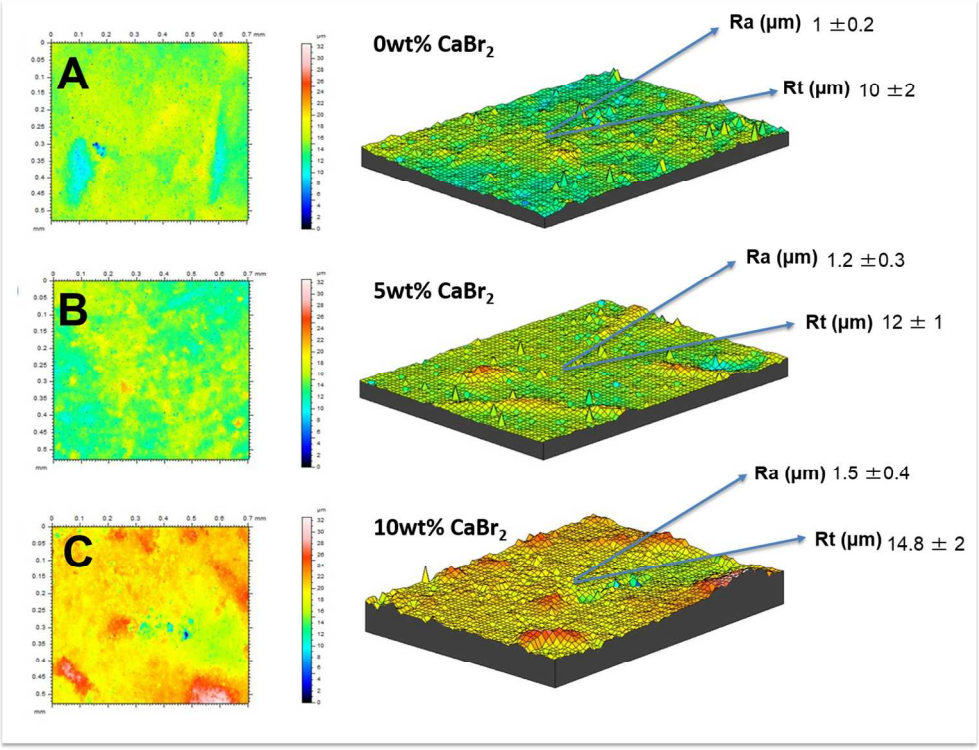

Figure 8. Ra, Rt roughness values, color map and 3D representation of surface roughness for 0, 5, and 10wt% CaBr2 doped 58S BG discs after thermal treatment up to 1150oC.

127x97mm (300 x 300 DPI)

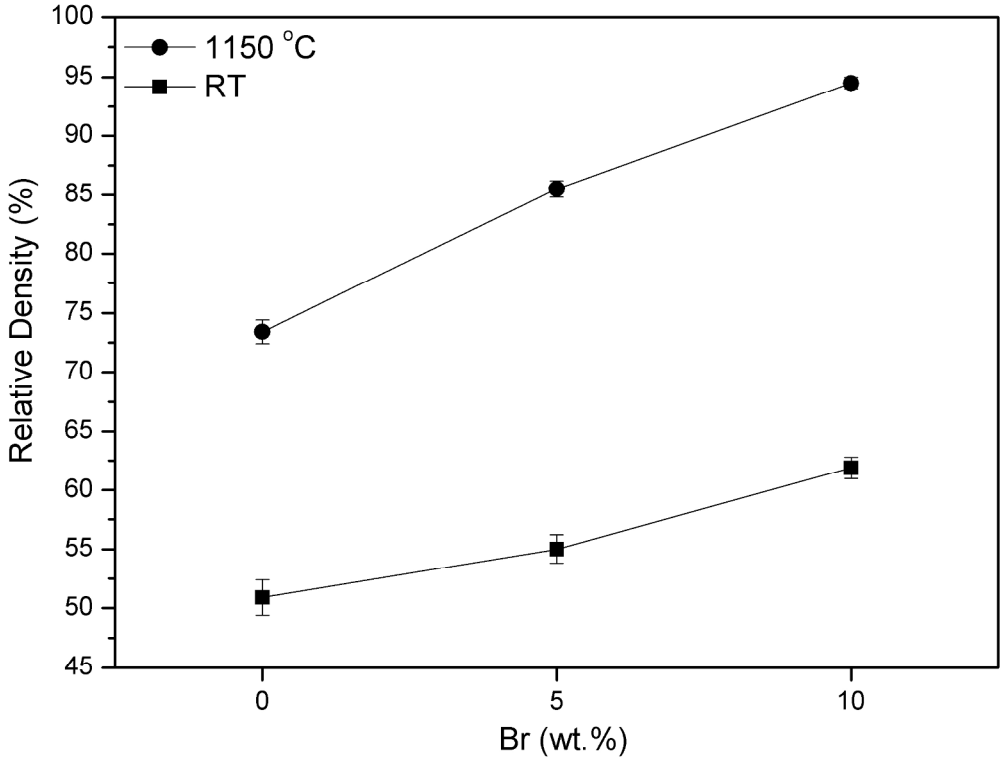

Figure 9. Relative densities of green and sintered discs of BG 58S containing or not 5wt% or 10wt% CaBr2.

225x171mm (300 x 300 DPI)

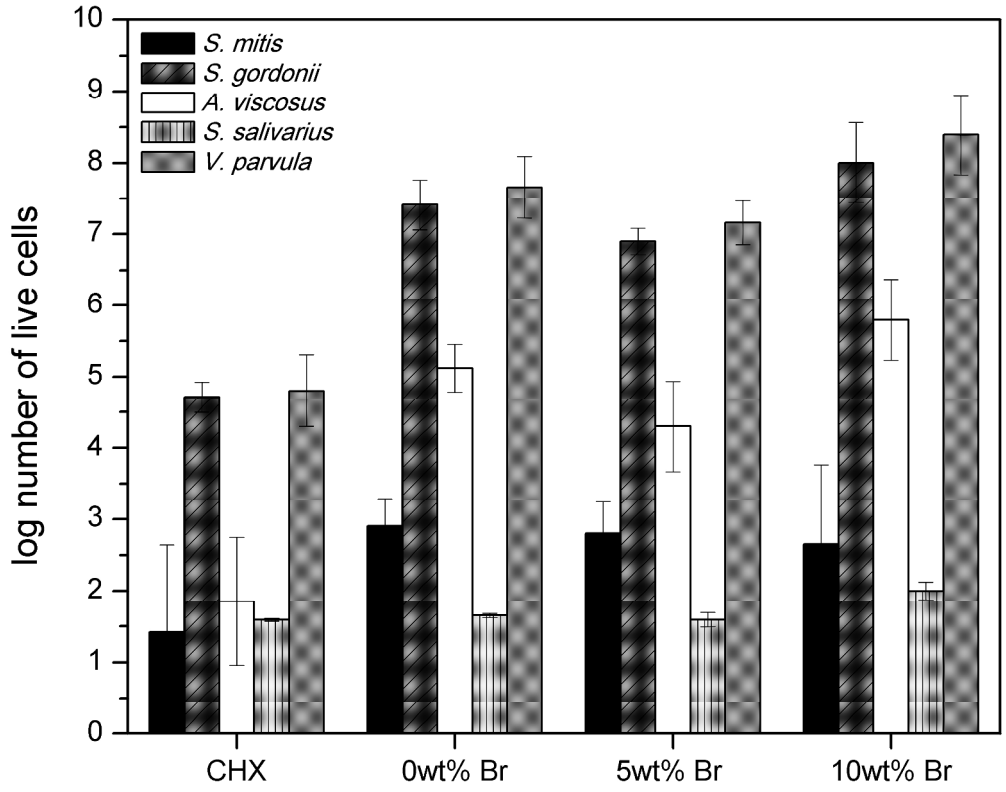

Figure 10. Inhibition of early and beneficial oral biofilm species on 0wt% CaBr2 58S BG discs with chlorhexidine (CHX) (positive control group), 0wt% CaBr2 BG58S discs (negative control group), 5 or 10 wt% CaBr2 BG58S discs.

259x208mm (300 x 300 DPI)

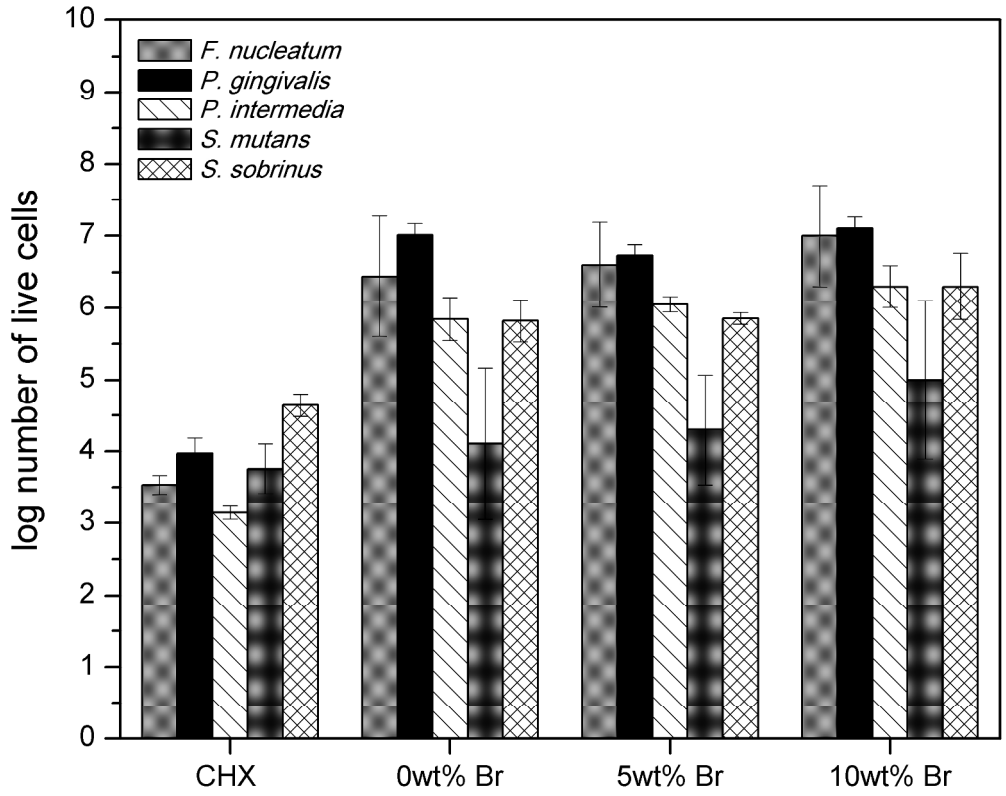

Figure 11. Inhibition of pathogen oral biofilm species on 0wt% CaBr2 BG58S discs with chlorhexidine (CHX) (positive control group), 0wt% CaBr2 BG58S discs (negative control group), and 5, 10 wt% CaBr2 BG58S discs.

259x210mm (300 x 300 DPI)

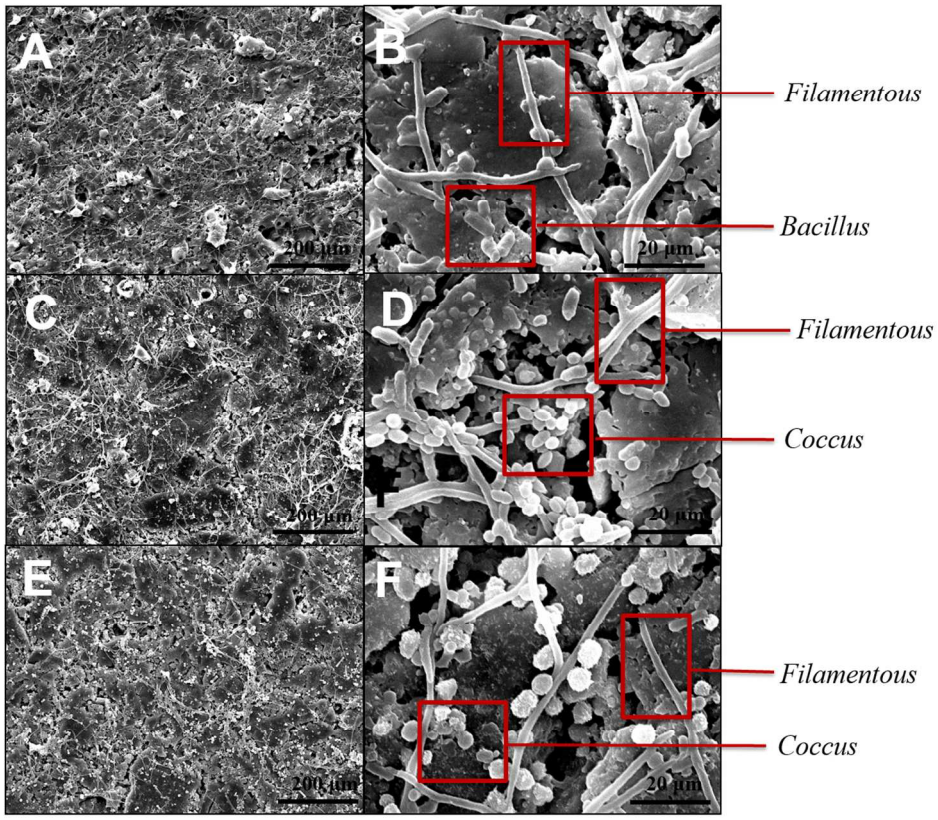

Figure 12. SEM images of multi-species biofilm adherence on BG58S discs with 0wt%CaBr2 (A,B), 5wt% CaBr2(C,D) and 10 wt% CaBr2(E,F).

115x98mm (300 x 300 DPI)